ChemPubSoc Europe

DOI: 10.1002/chem.201801444

CHEMISTRY A European Journal Full Paper

Fluorescent Probes

Highly Stable and Red-Emitting Nanovesicles Incorporating Lipophilic Diketopyrrolopyrroles for Cell Imaging

Antonio Ardizzone[+],[a] Davide Blasi[+],[a] Danilo Vona,[b] Arnulf Rosspeintner,[c] Angela Punzi,[b] Emiliano Altamura,[b] Natascia Grimaldi,[a] Santi Sala,[a] Eric Vauthey,[c] Gianluca M. Farinola,*[b] Imma Ratera,[a] Nora Ventosa,*[a] and Jaume Veciana*[a]

Abstract: Diketopyrrolopyrroles (DPPs) have recently attracted much interest as very bright and photostable red-emitting molecules. However, their tendency to form nonfluorescent aggregates in water through the aggregation-caused quenching (ACQ) effect is a major issue that limits their application under the microscope. Herein, two DPP molecules have been incorporated into the membrane of highly stable and water-soluble quatsomes (QS; nanovesicles composed of surfactants and sterols), which allow their nanostructuration in water and, at the same time, limits the ACQ effect. The obtained fluorescent organic nanoparticles showed superior structural homogeneity, along with long-term colloidal and optical stability. A thorough one- (1P) and two-photon (2P) fluorescence characterization revealed the promising photophysical features of these fluorescent nanovesicles, which showed a high 1P and 2P brightness. Finally, the fluorescent QSs were used for the in vitro bioimaging of Saos-2 osteosarcoma cell lines; this demonstrates their potential as nanomaterials for bioimaging applications.

Introduction

In recent decades, fluorescence microscopy has proven to be a powerful tool for visualizing and investigating biological systems. Advances in laser physics have determined the development of new microscopy techniques able to exploit both linear and nonlinear optical properties of the probes, which have improved several parameters, such as the lateral resolution of the images or the penetration depth into biological tissues.[1,2] The optimization of molecular structures to obtain probes with higher fluorescence quantum yield (QY), emission in the first or second biological transparency windows,[3] and intense one- or two-photon absorption (2PA)[4] cross sections usually lead to molecules with poor solubility in aqueous media, and therefore, with low potential concerning applications in microscopy.[5] A critical factor in the design of new bioimaging molecular probes is their tendency to aggregate in aqueous media with subsequent quenching of the emission; a phenomenon called aggregation-caused quenching (ACQ).[6] In recent years, several new molecular structures have been developed that show aggregation-induced emission (AIE);[7,8] a photophysical process in which molecules that do not fluoresce in solution became intense emitters upon organization into clusters or in the solid state, due to restriction of molecular motion upon aggregation. However, red/near-infrared (NIR) emission,[9,10] which is an important requirement to prevent the self-absorption of emitted light by tissues, is still an issue that requires complicated synthetic problems to be solved.[10]

Diketopyrrolopyrroles (DPPs) have recently been studied as fluorescent probes for bioimaging because of their high photostability and good fluorescence efficiency in the transparency window of biological tissues ($\lambda = 650$–900 nm).[11,12] Moreover, a number of reports have recently explored the 2PA properties of DPPs,[13,14] and showed their use as effective probes in two-photon (2P) fluorescence microscopy.[15,16] The large conjugated structure of the DPPs is responsible for their low water solubility and strong intermolecular interactions, which dramatically reduce their fluorescence QYs in aggregated states. Thus, chemical modification through the introduction of hydrophilic side chains on the DPP conjugated core has been used to obtain water-soluble probes.[17,18] Alternatively, in a few reported cases, water-insoluble DPP molecules have been processed as nanoparticles with a reduced ACQ effect, for application in in vitro and in vivo bioimaging.[16,19] In this context, and following our previous studies on the development of organometal-

[a] Dr. A. Ardizzone,[+] Dr. D. Blasi,[+] Dr. N. Grimaldi, Dr. S. Sala, Dr. I. Ratera, Dr. N. Ventosa, Prof. J. Veciana
Nanomol Department, Institut Ciencia Materials Barcelona (CSIC)-CIBER-BBN, Campus Universitari de Bellaterra
08193 Cerdanyola (Spain)
E-mail: ventosa@icmab.es
vecianaj@icmab.es

[b] D. Vona, Dr. A. Punzi, Dr. E. Altamura, Prof. G. M. Farinola
Dipartimento di Chimica
Università degli Studi di Bari Aldo Moro, Via Orabona 4, 70126 Bari (Italy)
E-mail: gianlucamaria.farinola@uniba.it

[c] Dr. A. Rosspeintner, Prof. E. Vauthey
Department of Physical Chemistry, University of Geneva
Quai Ernest Ansermet, 30, 1211 Geneve 4 (Switzerland)

[+] These authors contributed equally to this work.

Supporting information and the ORCID identification number for the author of this article can be found under: https://doi.org/10.1002/chem.201801444.

lic protocols for functionalized conjugated structures,[20–24] we recently published a study on the self-assembly process of several amphiphilic red-emitting DPP derivatives, with the formation of H and J aggregates in thin films and organic nanoparticles (ONPs).[25] Unfortunately, upon dispersion in water, all of these molecules show a severe ACQ effect, due to intense π–π stacking of the rigid conjugated structures. Herein, we present an alternative approach to disperse some of these water-insoluble molecules in aqueous media to limit the ACQ effects. This strategy consists of incorporating the DPP molecules inside the bilayer of quatsomes (QSs); an innovative class of nanovesicles.[26,27] QSs are highly stable nanovesicular structures made by quaternary ammonium surfactants with long alkyl chains, for example, cetyl trimethylammonium bromide (CTAB) and sterols, such as cholesterol (CHOL).[26,27] Such structures have recently been studied by some of us as alternative nanocarriers to liposomes, thanks to their outstanding stability and capability of multifunctional activity.[28–30] Moreover, we have also recently demonstrated that extremely stable and bright fluorescent organic nanoparticles (FONs) for bioimaging can be obtained by incorporating hydrophobic fluorenyl-derived fluorophores within QS membranes.[31] In these studies, it was shown that, upon incorporation in QSs, the fluorophores could be stably dispersed in water, which reduced the ACQ effect. Such dye-loaded QSs can be straightforwardly prepared in water through the self-assembly of surfactant, sterols, and dyes by means of the CO_2-based methodology of depressurization of an expanded liquid organic solution–suspension (DELOS-SUSP). Moreover, it has been shown that dispersions of QSs with superior vesicle-to-vesicle and membrane composition homogeneity can be obtained by DELOS-SUSP, in comparison with other conventional techniques for vesicle preparation.[27,28]

Herein, we aim to disperse in water, through incorporation in QSs, two water-insoluble DPPs molecules, **DPP-C8** and **DPP-C16** (Figure 1), which have been synthesized as reported in our previous work.[25] These molecules have the same conjugated backbone, and therefore, the same absorption and emission spectra (Figure 1 and the Supporting Information). They present the same hydrophilic part, which consists of triethylene glycol (TEG) chains at the two lactam nitrogen atoms, but differ in the length of the two terminal hydrophobic alkyl chains (C8 and C16) on both triazole rings. Such molecules were designed with the purpose of being anchored onto the QSs through interdigitation of the alkyl chains into the bilayer membranes, leaving the TEG chains exposed to the aqueous medium. Two different composition of QSs, made with CTAB and CHOL or cholesteryl hemisuccinate (CHEMS), with molar ratios of 1:1, were used to study the effect of QS composition on the stacking of DPPs within the membrane.

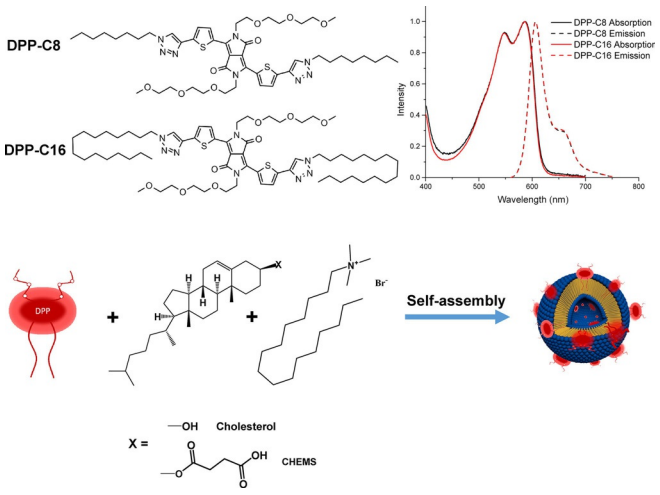

Figure 1. Top: Molecular structures of **DPP-C8** and **DPP-C16** (left) and their absorption and emission spectra in $CHCl_3$ (right). Bottom: Schematic representation of the formation of QSs with DPP molecules interdigitated in the bilayer of the vesicles.

Results and Discussion

Preparation and characterization of DPP-loaded QSs

Two samples of DPP-loaded QSs, namely, **QS-C8**, which contained **DPP-C8**, and **QS-C16**, which contained **DPP-C16**, were prepared in aqueous media by means of DELOS-SUSP with CHOL and CTAB in a 1:1 molar ratio (for further experimental details, see the Supporting Information). The two samples had the same fluorophore loading of $L = 0.6 \times 10^{-3}$, in which $L =$ moles dye/(mol CTAB + mol sterol) (for other studied samples in this work, see Table S1 in the Supporting Information).

CryoTEM micrographs of **QS-C8** and **QS-C16**, which were acquired one week and one month after preparation, are shown in Figure 2. The morphology (Figure 2) and size (Table S2 in the Supporting Information) of the **QS-C16** vesicles are very stable because no changes were observed during one month. On the contrary, only one week after the preparation of **QS-C8**, cryoTEM images provided evidence of the formation of small nanoaggregates with sheet/lamella twisted shapes at the edges, along with the presence of unilamellar nanovesicles. These nanoaggregates grew as rod-like architectures in a few weeks, with one dimension of a few nanometers and lengths up to several micrometers, showing the same behavior and aspect as

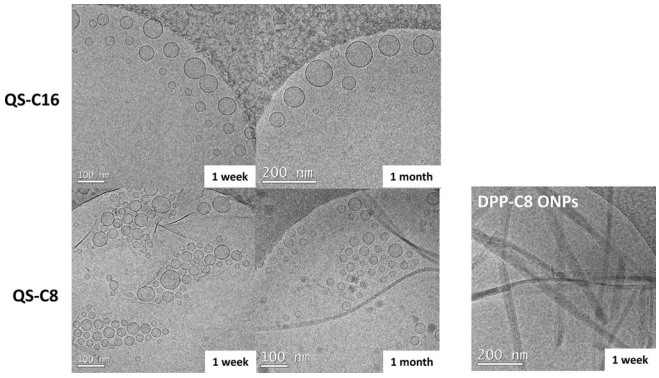

Figure 2. Left: CryoTEM micrographs of **QS-C16** (top) and **QS-C8** (bottom) recorded one week and one month after their preparation. Samples were stored at 4 °C under darkness. Right: CryoTEM micrographs of **DPP-C8** ONPs. The elongated nanoaggregates formed by **QS-C8** after one month are very similar to the structures appearing in **DPP-C8** ONPs after one week.

that of **DPP-C8** ONPs (Figure 2, bottom right), prepared by the reprecipitation method in water.[25] The changes in **QS-C8** are associated either with changes in the structure of the sheet/lamella nanoaggregates or with the labile anchoring of alkyl chains of the **DPP-C8** dye molecules to the QS membrane, and their release to the surrounding media in which supramolecular reorganization to nanorods occurs.

Changes in the morphology of **QS-C8** with time are also associated with variations in the band shape of the absorption spectrum (Figure S3, left, in the Supporting Information), with the appearance of a new band at $\lambda = 660$ nm due to the reorganization of the molecules and consequently the formation of new supramolecular aggregates.[25] Conversely, the absorption band shape of **QS-C16** (Figure S3, right, in the Supporting Information) did not show any significant changes, which indicated negligible reorganization and no release of the loaded dye molecules into the surrounding aqueous media. We observed that the presence of small fractions of EtOH (up to 10 vol%) in the water suspensions in which the **QS-C8** system was prepared stabilized the **QS-C8** vesicles, as revealed by CryoTEM micrographs and the absorbance spectra (Figure S4 in the Supporting Information). Thus, EtOH molecules are likely to solvate the DPP backbones, reducing the stacking interactions and enhancing the interdigitation of the aliphatic chains. The shape of the excitation spectrum (Figure S4 in the Supporting Information), which approaches the absorption profile, further supports this hypothesis. Notably, the length of the terminal alkyl chains plays a crucial role in the supramolecular organization and incorporation of the molecules into QSs in pure water. Indeed, C16 chains are long enough to ensure a strong interaction with the hydrophobic components of the QS bilayer; this stably anchors DPP molecules to the vesicles and enhances the stability of dye-decorated vesicles over time.

Nevertheless, in **QS-C16**, the stacking among probe molecules inside the membrane of QSs is only partially avoided. The mismatch between absorption and excitation spectra and the appearance of a nonemissive band at $\lambda = 660$ nm (Figure 3A), along with the low fluorescence QY (≈ 7%, as shown in Table 1)[32] compared with the dye in $CHCl_3$, indicate the formation of nonemissive aggregates, which suggests that the observed residual emission is only due to isolated molecules

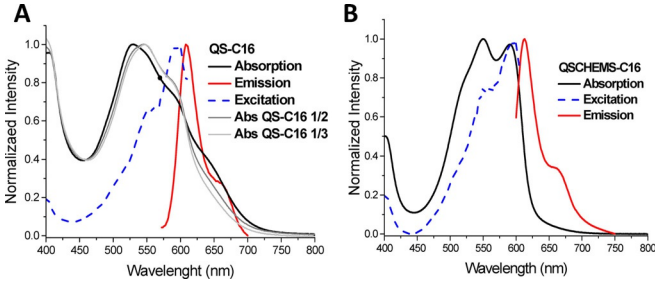

Figure 3. A) Normalized absorption, emission, and excitation spectra of **QS-C16**. Normalized absorption spectra of QS at lower loadings of **DPPC16** (**QS-C16 1/2** and **QS-C16 1/3**) are also shown. B) Normalized absorption, emission, and excitation spectra of **QSCHEMS-C16**. In this case, the absorption spectrum, which is more similar to that of the molecule in solution, suggests a lower presence of aggregates within the vesicle membranes.

Table 1. Estimated values of fluorescence QYs [%] for nano-objects studied herein.

	DPP-C16 ($CHCl_3$)	QS-C16	QS-C16 (1/2)	QS-C16 (1/3)	QSCHEMS-C16
QY[a]	70	7	13	18	41

[a] Calculated at the maximum excitation wavelength of the **DPP-C16**-loaded QSs in water relative to the dye in $CHCl_3$.

within the membrane. Notably, the excitation and emission band shapes of **DPP-C16** dissolved in an organic solvent and dispersed in the vesicle membranes are identical; this indicates that isolated **DPP-C16** molecules exclusively contribute to the emission of QS-based samples. Derivative **QS-C16** was much brighter than other dispersions (alternative to vesicle membrane hosting) of the same dye in water, such as **DPP-C16** ONPs, which were prepared by reprecipitation. The ONPs of **DPP-C16** showed a fluorescence QY of < 0.1%, despite a desirable NIR emission (Figure S5 in the Supporting Information); this was attributed to the formation of fluorescent J aggregates within the nanoparticles.

To verify the formation of nonfluorescent aggregates inside the bilayers of **QS-C16**, two samples loaded with one-half (**QS-C16** (1/2), with $L = 0.3 \times 10^{-3}$) and one-third (**QS-C16** (1/3), with $L = 0.2 \times 10^{-3}$) of **DPP-C16** were prepared. As shown in Figure 3A, the slight changes in the absorption band shape, such as a decrease in the band at $\lambda = 660$ nm and an increase at $\lambda =$ 590 and 550 nm, as well as the increase in the fluorescence QY (up to 18% for **QS-C16** (1/3)) suggest that more dye molecules are distributed as isolated molecules over the membrane of the vesicles at lower loadings. (Dye loading in the QS membrane was measured by means of UV/Vis absorption by following the procedure described in the Supporting Information (section on sample preparation).)

Because the principle of obtaining bright FONs in water is to confine a high number of bright dye molecules in a small volume, we tested whether the composition of QSs had an effect on the number of aggregated dye molecules incorporated in the membrane of the vesicles responsible for the detrimental ACQ effect. Thus, the **DPP-C16**-loaded sample of the QSs containing CHEMS (**QSCHEMS-C16**) with the same loading $L = 0.6 \times 10^{-3}$) as that of **QS-C16** were prepared by means of DELOS-SUSP, with the expectation that the larger size and hydrophilic carboxylic acid head groups of CHEMS molecules would modify the incorporation of DPP molecules and their aggregation in the membrane. The resulting nanovesicles were smaller than that of **QS-C16** (around 55 nm, as shown in Table S2 in the Supporting Information) and they were found to be highly stable in terms of morphology, size, and optical properties (Figure S7 and Table S2 in the Supporting Information). Notably, sample **QSCHEMS-C16** showed the highest fluorescence efficiency (QY ≈ 41%; Table 1) among the studied nanostructures, which proved, along with the shapes of the spectra shown in Figure 3B, that the probe molecules were significantly less aggregated in the bilayer in this formulation than that in **QS-C16**. This is likely to be due to the hydrophilici-

ty and bulkier size of the CHEMS group than that of CHOL in **QS-C16**, which may hinder π–π stacking between the probes. In comparison to **QS-C16**, sample **QSCHEMS-C16** leads to a huge gain in brightness because these FONs have an approximately 6 times higher efficiency in a volume that is $<20\,\%$ of the **QS-C16**. These features make **QSCHEMS-C16** highly promising candidates as red-emitting nanoprobes for in vivo and in vitro bioimaging.

Because DPP molecules are effective probes in 2P fluorescence microscopy, which is beneficial for bioimaging applications, we decide to characterize the 2P absorption properties of DPP-loaded QSs in water. The 2P spectra and 2P brightness of **DPP-C16** and **DPP-C16**-loaded QSs were determined by means of the two-photon excited fluorescence (TPEF) technique (see the Supporting Information), the results of which are shown in Figure 4.

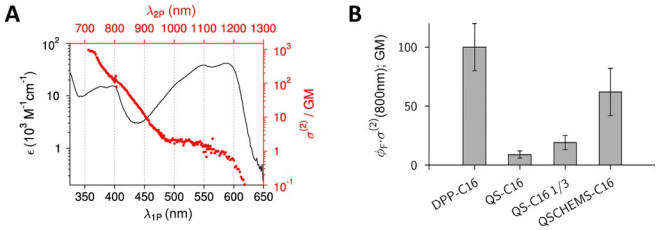

Figure 4. Left: The one-photon (1P; black) and 2P (red) cross-sectional spectra of **DPP-C16** in $CHCl_3$. Right: The 2P brightness at $\lambda = 800$ nm of **DPP-C16** in $CHCl_3$ and the corresponding DPP-loaded QSs in water.

Figure 4A compares the 1P and 2P absorption spectra of **DPP-C16** in $CHCl_3$, which differ considerably from each other; a common feature for quadrupolar molecules.[33] Although the lowest energy transition (peaking at around $\lambda \approx 590$ nm) is strongly 1P allowed, it is almost completely 2P forbidden (with $\sigma^{(2)}$ values of well below 10 GM). However, the 2P cross section increases significantly below $\lambda = 950$ nm, up to a value of about 1000 GM at $\lambda = 710$ nm. These results are in good agreement with data from a similar series of DPP compounds.[34]

In agreement with previous results on 1P characterization, the 2P excitation spectra of **DPPC-16** in $CHCl_3$ and **DPP-C16**-loaded QSs in water are identical (Figure S8 in the Supporting Information). The absolute invariance of all spectral properties of the emissive species corroborates our abovementioned assumption that at least part of the dye is incorporated into the QSs not in the form of aggregates, but rather as single, unperturbed dye molecules. We emphasize that the 2P excitation method only allows for observing 2P cross sections of species that show emissions. Thus, potential 2P absorption from the nonemissive aggregates is, of course, not visible. To obtain a useful quantity, in terms of practical applications, we decided to present the 2P brightness of the QS samples, $\sigma^{(2)}\cdot QY$ (or $\sigma^{(2)}\cdot\phi_F$), at $\lambda = 800$ nm as a figure of merit (FOM). Figure 4B shows clearly that the 2P brightness decreases strongly for the conventional QS samples, most probably because the concentration of single emissive dyes is lower in QSs. The highest value of the FOM, by far, is achieved for **QSCHEMS-C16** (in agreement with the 1P photophysical characterization), which, thanks to the small volume, is an attractive probe for 2P microscopy and worthy to be studied in more detail. A point worth mentioning is that, due to the confinement, and thus, higher local concentration of dyes in the QS, the brightness per nm^3 is orders of magnitude better than that for a homogeneous distribution of pure dyes because of the higher local concentration of dyes attained.

Biocompatibility assays of DPP-loaded QSs and DPP ONPs

Because the main interest for studying DPP-loaded QSs is their use as florescent probes for bioimaging, we performed cell viability and growth studies. Thus, biocompatibility assays for **DPP-C16** ONPs, **QS-C16**, and **QSCHEMS-C16** were performed on the Saos2 cell line because it is an adherent model cell line used for osteoblast adhesion tests (in biomaterial research)[35,36] or for an osteosarcoma in vitro model for drug testing (in anticancer research).[37] For the biocompatibility assays of the novel FONs reported herein, the cells were first precultured for 24 h to allow adhesion, then exposed to the sample solutions for 4 h, and finally recultured in fresh medium for 36 h.[38] After preliminary 3-(4,5-dimethylthiazol-2-yl)-2,5-diphenyltetrazolium bromide (MTT) tests, two concentrations (1 and 10 nM, related to dye concentration in formulation) per sample were tested in triplicate. MTT analysis was performed to measure the metabolic activity of Saos2 cells, that is, to analyze cell viability and predict growth. As positive growth controls, we used cells without exposition to sample solutions and grown onto polystyrene wells. MTT assays for these samples were recorded after 10 min of seeding (PSCC(0)) and after 36 h (PSCC*). A complete comparison was also performed on single dye-free formulations, such as CTAB only, plain QSs with CHOL, and plain QSs with CHEMS (Figure 5). Cytotoxicity was detected for plain QSs in a weakly dose-dependent manner. Because Saos2 cells are sensitive to CTAB in the range of 0.2–2 mM, samples at lower concentration of CTAB, 7 and 0.7 μM, were tested, cor-

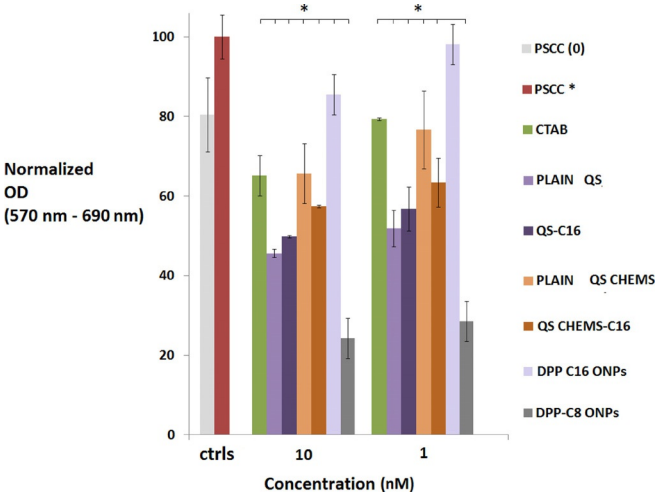

Figure 5. PSCC*-normalized MTT values for biocompatibility assays. Data were statistically validated by means of an analysis of variance (ANOVA) test/Bonferroni post-test (evaluation of correlation PSCC* for each sample with a significance of $p < 0.05$).

responding to probe concentrations of 10 and 1 nM, respectively.[39] Other cell types, such as HeLa cells, exhibit a decrease in cell viability only at higher concentrations of different quaternary ammonium surfactants.[40] Plain QS are more cytotoxic than that of CTAB, but plain CHEMS QSs are slightly less cytotoxic than both CTAB and plain QSs. There is no statistically relevant effect due to the dye in loaded QSs (**QS-C16** and **QS CHEMS-C16**), with respect to unloaded QS (both plain QSs and **QSCHEMS**); all FONs containing CHEMS exhibit a relatively good biocompatibility (≈60–73%) that is allowable, in principle, for in vivo studies. All tested QSs made from CHOL/CTAB exhibit a relatively good biocompatibility (<60%). Therefore, CHEMS has an ameliorative effect on the biocompatibility of the composition. The ONPs of **DPP-C16** exhibit the best biocompatibility, in terms of absence of metabolic distress (in correlation with PSCC*) and absence of cell death related to starting cell density (PSCC(0)). The ONPs of **DPP-C8** are strongly toxic at the two tested concentrations (relative biocompatibility <30%). The biocompatibility of **QS-C8** was not tested because of its low morphological stability in the absence of EtOH, as mentioned above.

Cellular uptake assays of DPP-C16 ONPs, QS-C16, and QSCHEMS-C16

Cellular uptake assays were performed for **DPP-C16** ONPs and the two different QS formulations, **QS-C16** and **QSCHEMS-C16**, at concentrations of 10 and 1 nM (related to dye concentrations) in experiments at 1 and 4 h exposition times with different staining agents (for staining protocols, see the Supporting Information). The best results were obtained at 1 h (Figure 6). In the case of **DPP-C16** ONPs, a 1 nM concentration of dye was effective (with 10 nM cells gave weak/low uptake). Vesicles of **QS-C16** were not taken up at 1 and 10 nM, whereas for **QSCHEMS-C16** a concentration of 10 nM was necessary (no uptake was detected at 1 nM). DAPI staining was performed to verify the absence of nuclei fragmentation or any other nuclear anomaly, whereas actin fiber stress staining with ATTO 488 was performed to investigate cell adhesion and interaction with the substrate.

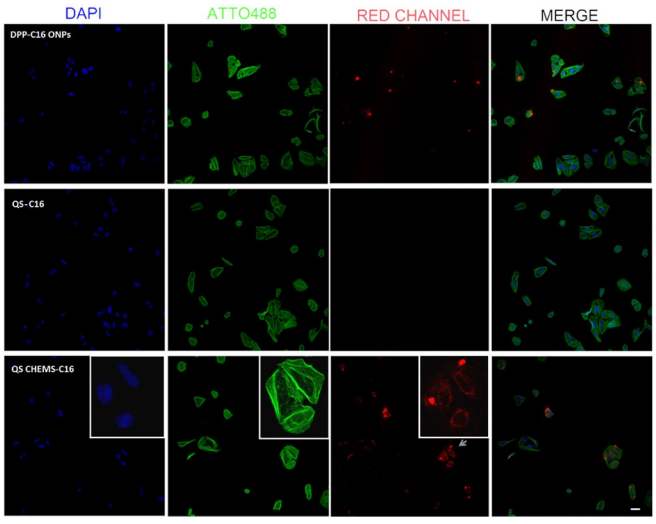

Figure 6. Confocal microscopy images of 4′,6-diamidino-2-phenylindole (DAPI)/Phalloidin-ATTO 488/DPP probe (**QS-C16** ONPs, **QS-C16**, or **QSCHEM-C16**; red channel). Staining for the three samples 1 h after uptake of 1 nM **DPP-C16** ONPs or 10 nM of both **QS-C16** and **QS CHEM-C16**. Marker: 50 μm.

After 1 h exposition to **DPP-C16** ONPs (1 nM), actin stress fibers are generally morphologically well present in all samples and nuclei are unaltered. Strongly red-emitting aggregates of **DPP-C16** ONPs were observed inside the cells, but not outside them. The average size of the aggregates after 1 h was determined by means of image analysis as (5.1±0.9) μm. After 4 h, ONPs were smaller and more sporadic. The staining seems to result from a combination of both incorporation and aggregation inside cells, and is not homogeneous. In 40% of acquired images, the **DPP-C16** ONP uptake is perinuclear and produces small aggregates in the cytoplasm and around the membrane (Figure 7, left). Concerning **QS-C16** (10 nM) at 1 h, concentric

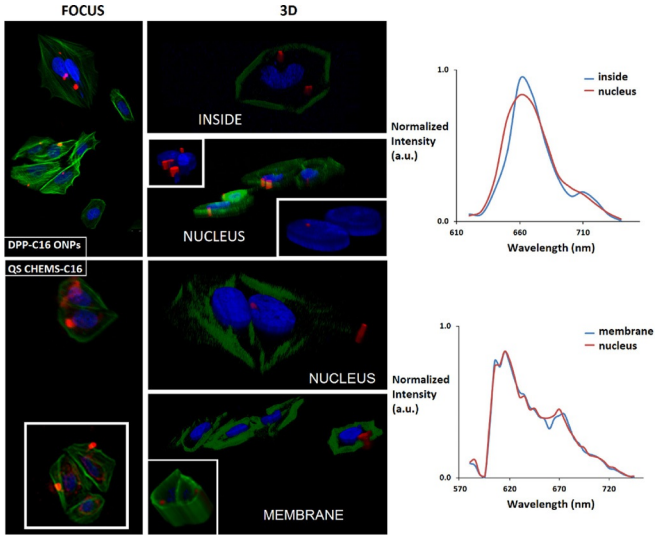

Figure 7. Left: Confocal microscopy images of DAPI/Phalloidin-ATTO 488/DPP staining of **DPP-C16** ONPs and **QSCHEM-C16** samples 1 h after uptake together with 3D reconstructions for different DPP localization. Right: Emission spectra obtained through the confocal approach of fluorescent aggregates of **DPP-C16** from **DPP-C16** ONP stained cells (top) and **QSCHEMS-C16**-stained cells (bottom).

fibers were observed in many cells; this may be due to negative cell stress, whereas nuclei staining reveals no fragmentation. However, there is no evidence of cellular uptake (neither after 4 h nor at lower concentration). On the other hand, in the case of **QSCHEMS-C16**, actin stress fibers are generally morphologically well present in all samples, although there are also concentric stress fibers for some unfavorable conditions. The DAPI channel reveals good morphology of nuclei. Uptake of **QSCHEMS-C16** appears to be complex: there is a general spread of cytoplasmic staining, with perinuclear and membrane/cytoplasm specific formation of strongly red-emitting aggregates ((8.1±2.8) μM at 1 h), which in a few cases are also localized outside the cells. Staining completely disappeared after 4 h.

Confocal images of DAPI/Phalloidin-ATTO 488/DPP staining of **DPP-C16** ONPs and **QSCHEM-C16** uptake after 1 h with 3D reconstructions are shown in Figure 7. For **DPP-C16** ONPs, small clusters in the nuclear and perinuclear regions were observed (see below), some of them were localized inside the cells, maybe in the cytoplasm. In the case of **QSCHEMS-C16**, the simultaneous nonspecific spread of staining of the cytoplasm, along with membrane and nuclear regions, was detected. In situ emission spectra recorded in combination with confocal microscopy was only performed for small clusters located in different cell regions. In the case of **DPP-C16** ONPs, emission spectra in the two stained regions, around the nuclei and cytoplasm, are slightly different (Figure 7, top right). The fluorescence signal of the aggregates shows a small shoulder in the NIR region, at $\lambda \approx 710$ nm, which can be associated with the weak emission of the **DPP-C16** ONPs (see Figure S3 in the Supporting Information). The main band at $\lambda = 660$ nm can be ascribed to emission from isolated molecules of **DPP-C16**; this is likely to be due to the deaggregation of the nanoparticles, maybe as an effect of the interaction with cellular proteins. In the case of **QSCHEMS-C16**, spectra taken from clusters localized on the cell membrane and nuclear region are similar to those acquired in water (see Figure 4); this is likely to indicate that probe molecules are maintained inside QS CHEMS, even after incorporation into cells (Figure 7, bottom right). In summary, it appears that **QSCHEMS-C16** is the best FON for interaction with DPP derivatives for bioimaging applications. These fluorescent vesicles show a good uptake by cells and maintain their structures inside the cells.

Conclusions

Non-water-soluble DPPs, modified with two C8 or C16 alkyl tails (**DPP-C8** and **DPP-C16**, respectively), have been dispersed in water by incorporating them in the membrane of QSs, which are nanovesicles that are highly stable in water, in such a way that the alkyl tails of the dyes are interdigitated within the membrane of the vesicles. The alkyl chain length plays a crucial role in the stability of the obtained fluorescent vesicles; the C16 chains ensure stable anchoring of the dye to the membrane of the vesicles (**QS-C16**). The 1P and 2P photophysical characterizations indicated that the presence of nonfluorescent aggregates (ACQ effect) of **DPP-C16** strictly depended on the dye loading, *L*, that is, the amount of dye per amount of QSs components, and the composition of the vesicles. DPP-loaded QSs composed of hemisuccinate-modified CHOL and CTAB (**QSCHEMS-C16**) showed the lowest ACQ effect and highest fluorescence efficiency (QY $\approx$ 41 %), which suggested the presence of isolated fluorophore molecules within the membrane of the vesicles. The attractive physicochemical and optical properties of DPP-loaded QSs encouraged the application of such probes for in vitro cells imaging. Biological assays showed that DPP-loaded QSs were not cytotoxic at the concentrations required for the fluorescence imaging of the Saos-2 cell line. Confocal images and in situ emission spectra showed that **QSCHEMS-C16** was successfully taken up by cells, without undergoing structural modification. The results described demonstrate that DPP-loaded QSs are promising candidates as nanoprobes for further studies, such as the imaging of living organisms, in which red-emitting probes are required, or the synthesis of multifunctional vesicles, by incorporating additional active molecules, for theranostic applications.

Experimental Section

Experimental details on the preparation and characterization of samples, and on biological assays, are given in the Supporting Information.

Acknowledgements

This work was financially supported by the DGI, Spain (Grant MOTHER; MAT2016-80826-R); AGAUR, Generalitat de Catalunya (Grant 2017 SGR 918); and the Networking Research Center on Bioengineering, Biomaterials, and Nanomedicine (CIBER-BBN). Part of the characterization work has been performed by the ICTS "NANBIOSIS", at the Biomaterial Processing and Nanostructuring Unit #6 of the CIBER in Bioengineering, Biomaterials & Nanomedicine (CIBER-BBN). D.B. and A.A. acknowledge the European Commission (EC) FP7-PEOPLE-2013-Initial Training Networks (ITN) "NANO2FUN" project no. 607721 for their predoctoral contracts. This work was also supported by the Ministero dell'Istruzione, dell'Università e della Ricerca (MIUR; Progetto PRIN 2012 prot. 2012A4Z2RY and Project PON02_00563_3316357 (PON MAAT)). Financial support from the Fonds National Suisse de la Recherche Scientifique (no. 200020-165890) and the University of Geneva is also acknowledged.

Conflict of interest

The authors declare no conflict of interest.

Keywords: aggregation · fluorescence · imaging agents · nanoparticles · vesicles

[1] S. W. Hell, *Nat. Biotechnol.* **2003**, *21*, 1347 – 1355.
[2] F. Helmchen, D. W. Winfried, *Nat. Methods* **2005**, *2*, 932 – 940.
[3] E. Hemmer, A. Benayas, F. Légaré, F. Vetrone, *Nanoscale Horiz.* **2016**, *1*, 168 – 184.
[4] H. M. Kim, B. R. Cho, *Chem. Rev.* **2015**, *115*, 5014 – 5055.
[5] S. Luo, E. Zhang, Y. Su, T. Cheng, C. Shi, *Biomaterials* **2011**, *32*, 7127 – 7138.
[6] A. Kaeser, A. P. H. J. Schenning, *Adv. Mater.* **2010**, *22*, 2985 – 2997.
[7] J. Mei, Y. Hong, J. W. Lam, A. Qin, Y. Tang, B. Z. Tang, *Adv. Mater.* **2014**, *26*, 5429 – 5479.
[8] K. Mandal, D. Jana, B. K. Ghorai, N. R. Jana, *J. Phys. Chem. C* **2016**, *120*, 5196 – 5206.
[9] J. Zhang, A. Liu, X. B. Pan, L. Yao, L. Wang, J. Fang, J. Wu, *ACS Appl. Mater. Interfaces* **2015**, *7*, 26266 – 26274.
[10] A. L. Antaris, *Nat. Mater.* **2015**, *15*, 235 – 242.
[11] M. Kaur, D. H. Choi, *Chem. Soc. Rev.* **2015**, *44*, 58 – 77.
[12] Y. Qua, Y. Wua, Y. Gao, S. Qub, L. Yang, J. Hua, *Sensor. Actuat. Chem. B* **2014**, *197*, 13 – 19.
[13] Z. E. H. Ghazvini, M. V. M. Bondar, K. D. Belfield, *J. Phys. Chem. C* **2015**, *119*, 8864 – 8875.

[14] A. Nowak-Król, M. Grzybowski, J. Romiszewski, M. Drobizhev, G. Wicks, M. Chotkowski, A. Rebane, E. Gorecka, D. T. Gryko, *Chem. Commun.* **2013**, *49*, 8368 – 8370.
[15] D. Chandran, K.-S. Lee, *Macromol. Res.* **2013**, *21*, 272 – 283.
[16] Y. Gao, G. Feng, T. Jiang, C. Goh, L. Ng, B. Liu, B. Li, L. Yang, J. Hua, H Tian, *Adv. Funct. Mater.* **2015**, *25*, 2857 – 2866.
[17] E. Heyer, P. Lory, J. Leprince, M. Moreau, A. Romieu, M. Guardigli, A. Roda, R. Ziessel, *Angew. Chem. Int. Ed.* **2015**, *54*, 2995 – 2999; *Angew. Chem.* **2015**, *127*, 3038 – 3042.
[18] M. Grzybowski, E. Glodkowska-Mrowka, V. Hugues, W. Brutkowski, M. Blanchard-Desce, D. T. Gryko, *Chem. Eur. J.* **2015**, *21*, 9101 – 9110.
[19] K. Pu, J. Mei, J. V. Jokerst, G. Hong, A. L. Antaris, N. Chattopadhyay, A. J. Shuhendler, T. Kurosawa, Y. Zhou, S. S. Gambhir, Z. Bao, J. Rao, *Adv. Mater.* **2015**, *27*, 5184 – 5190.
[20] A. Punzi, M. A. M. Capozzi, V. Fino, C. Carlucci, M. Suriano, E. Mesto, E. Schingaro, E. Orgiu, S. Bonacchi, T. Leydecker, P. Samorì, R. Musio, G. M. Farinola, *J. Mater. Chem. C* **2016**, *4*, 3138 – 3142.
[21] A. Punzi, F. Nicoletta, G. Marzano, C. G. Fortuna, J. Dagar, T. M. Brown, G. M. Farinola, *Eur. J. Org. Chem.* **2016**, 3233 – 3242.
[22] M. C. Tanese, G. M. Farinola, B. Pignataro, L. Valli, L. Giotta, S. Conoci, P. Lang, D. Colangiuli, F. Babudri, F. Naso, L. Sabbatini, P. G. Zambonin, L. Torsi, *Chem. Mater.* **2006**, *18*, 778 – 784.
[23] G. M. Farinola, V. Fiandanese, L. Mazzone, F. Naso, *J. Chem. Soc. Chem. Commun.* **1995**, *24*, 2523 – 2524.
[24] A. Punzi, D. I. Coppi, S. Matera, M. A. M. Capozzi, A. Operamolla, R. Ragni, F. Babudri, G. M. Farinola, *Org. Lett.* **2017**, *19*, 4754 – 4757.
[25] A. Punzi, E. Maiorano, F. Nicoletta, D. Blasi, A. Ardizzone, N. Ventosa, I. Ratera, J. Veciana, G. M. Farinola, *Eur. J. Org. Chem.* **2016**, 2617 – 2627.
[26] L. Ferrer-Tasies, E. Moreno-Calvo, M. Cano-Sarabia, M. Aguilella-Arzo, A. Angelova, S. Lesieur, S. Ricart, J. Faraudo, N. Ventosa, J. Veciana, *Langmuir* **2013**, *29*, 6519 – 6528.
[27] E. Elizondo, J. Larsen, N. S. Hatzakis, I. Cabrera, T. Bjørnholm, J. Veciana, D. Stamou, N. Ventosa, *J. Am. Chem. Soc.* **2012**, *134*, 1918 – 1921.
[28] I. Cabrera, E. Elizondo, O. Esteban, J. L. Corchero, M. Melgarejo, D. Pulido, A. Córdoba, E. Moreno, U. Unzueta, E. Vazquez, I. Abasolo, S. Schwartz, Jr., A. Villaverde, F. Albericio, M. Royo, M. F. García-Parajo, N. Ventosa, J. Veciana, *Nano Lett.* **2013**, *13*, 3766 – 3774.
[29] I. Cabrera, I. Abasolo, J. L. Corchero, E. Elizondo, P. R. Gil, E. Moreno, J. Faraudo, S. Sala, D. Bueno, E. González-Mira, M. Rivas, M. Melgarejo, D. Pulido, F. Albericio, M. Royo, A. Villaverde, M. García-Parajo, S. Schwartz, Jr., N. Ventosa, J. Veciana, *Adv. Healthcare Mater.* **2016**, *5*, 829 – 840.
[30] N. Grimaldi, F. Andrade, N. Segovia, L. Ferrer-Tasies, S. Sala, J. Veciana, N. Ventosa, *Chem. Soc. Rev.* **2016**, *45*, 6520 – 6545.
[31] X. Liu, A. Ardizzone, B. Sui, M. Anzola, N. Ventosa, T. Liu, J. Veciana, K. D. Belfield, *ACS Omega* **2017**, *2*, 4112 – 4122.
[32] C. Würth, M. Grabolle, J. Pauli, M. Spieles, U. Resch-genger, *Nat. Protoc.* **2013**, *8*, 1535 – 1550.
[33] C. Katan, F. Terenziani, O. Mongin, M. H. V. Werts, L. Porrès, T. Pons, J. Mertz, S. Tretiak, M. Blanchard-Desce, *J. Phys. Chem. A* **2005**, *109*, 3024 – 3037.
[34] A. Purc, K. Sobczyk, Y. Sakagami, A. Ando, K. Kamada, D. T. Gryko, *J. Mater. Chem. C* **2015**, *3*, 742 – 749.
[35] E. M. Czekanska, M. J. Stoddart, R. G. Richards, J. S. Hayes, *Eur. Cells Mater.* **2012**, *24*, 1 – 17.
[36] P. Müller, U. Bulnheim, A. Diener, F. Lüthen, M. Teller, E. D. Klinkenberg, H. G. Neumann, B. Nebe, A. Liebold, G. Steinhoff, J. Rychly, *J. Cell. Mol. Med.* **2008**, *12*, 281 – 291.
[37] H. Ma, C. He, Y. Cheng, Z. Yang, J. Zang, J. Liu, X. Chen, *ACS Appl. Mater. Interfaces* **2015**, *7*, 27040 – 27048.
[38] S. R. Cicco, D. Vona, R. Gristina, E. Sardella, R. Ragni, M. Lo Presti, G. M. Farinola, *Bioengineering* **2016**, *3*, 35 – 54.
[39] M. Kalbácová, M. Verdánová, F. Mravec, T. Halasová, M. Pekar, *Colloids Surf. A* **2014**, *460*, 204 – 208.
[40] N. Vlachy, D. Touraud, J. Heilmann, W. Kunz, *Colloids Surf. B* **2009**, *70*, 278 – 280.

Manuscript received: March 21, 2018
Revised manuscript received: May 28, 2018
Accepted manuscript online: June 5, 2018
Version of record online: July 3, 2018